Transport-Number Determination of a Protonic Ceramic Electrolyte Membrane via Electrode-Polarisation Correction with the Gorelov Method

Domingo Pérez-Coll[a], Gemma Heras-Juaristi[a], Duncan P. Fagg[b], Glenn C. Mather[a*]

[a]*Instituto de Cerámica y Vidrio, CSIC, Cantoblanco, 28049 Madrid, Spain*
[b]*Nanotechnology Research Division, Centre of Mechanical Technology and Automation, Department of Mechanical Engineering, University of Aveiro, 3810-193, Aveiro, Portugal*

*e-mail address: mather@icv.csic.es
Tel.: + 34 917355840
Fax.: + 34 917355843

Abstract

Analysis of transport numbers is critical for assessing the suitability of an ion-conducting material for a given electrochemical application and the conditions for its employment. In this work, the proton, oxide-ion and electron transport numbers of the candidate protonic ceramic electrolyser and fuel cell material $SrZr_{0.9}Y_{0.1}O_{3-\delta}$ (with the addition of 4 mol% ZnO as sintering aid) are measured in wet and dry oxidising atmospheres in the temperature range 700-850 °C. The determination of proton transport numbers is analysed in detail, encompassing the suitability of equivalent circuits in different conditions and the inclusion of an external parallel resistance for the correction of electrode-polarisation effects (Gorelov method). It is confirmed that transport numbers are highly inaccurate if no polarisation correction is applied. In dry oxidising conditions oxide-ion transport numbers, t_o, lie in the range 0.63–0.78. The conductivity in wet oxidising conditions is dominated by protons and an electronic component, with the proton transport number increasing from 0.79 to 0.88 with increasing pH_2O in the range $1.1x10^{-3} \leq pH_2O \leq 1.27x10^{-2}$ atm at 700 ºC.

Keywords: strontium zirconate, proton conduction, solid oxide electrolyser cell, modified electromotive force technique, transference number, protonic ceramic fuel cell

1. Introduction

One of the most important energy vectors of the future for motive power, stationary-energy needs and portable electronics is likely to be hydrogen [1-4]. Presently, many large and growing industrial processes also require this fuel as a reactant, which currently is mostly extracted from dwindling hydrocarbon sources. Alternative production methods, which are both sustainable and environmentally benign, are thus very necessary in the medium term.

Pure, dry hydrogen required for power in fuel cells and certain industrial applications may be produced efficiently in a high temperature range 600 – 900 °C through the electrolysis of steam employing a ceramic proton-conducting membrane [5,6]. Such protonic ceramic electrolyser cells (PCECs) conduct protons through a dense oxide, typically a stable perovskite membrane, evolving hydrogen at the cathode. In contrast to an oxide-ion-conducting membrane (SOEC, solid oxide electrolyser cell), the produced hydrogen does not need to be separated from reactant steam. The study of PCECs is still in its infancy, although $SrZrO_3$-based phases have emerged as very strong candidates for this application due to their good chemical and mechanical stability in comparison to other perovskite proton conductors [5,7]. These advantages of $SrZrO_3$ suggest that, despite its more moderate conductivity than competitor perovskite proton conductors such as $BaZrO_3$- and $BaCeO_3$-based phases [8], it may also be employed as electrolyte in protonic ceramic fuel cells (PCFCs) in a thin-film configuration.

The determination of transport numbers of ion-conducting ceramics for electrolysers, fuel cells and related electrochemical devices is of considerable interest for evaluating both their suitability for application and performance. In the case of PCECs, a high proton-transport number is required to maximize the current efficiency of steam electrolysis. Protons are incorporated in wet conditions as a result of acceptor

doping on the B site of the perovskite, with a hydroxyl group and a proton from an ambient water molecule replacing an oxygen vacancy, $V_o^{\bullet\bullet}$

$$H_2O + O_O^x + V_O^{\bullet\bullet} \rightleftarrows 2OH_O^{\bullet} \quad (1)$$

In dry atmospheres and high temperatures water is desorbed, resulting in the formation and migration of oxygen vacancies. Alternatively, the oxygen vacancies may be compensated in oxidising atmospheres by the formation of electron holes.

The range of operation of an electrolyte material is limited by the electrolytic domain, whereas the joint diffusion of protonic defects and oxide-ion vacancies gives rise to the transport of water vapour in a chemical potential gradient of steam [9]. This is undesirable for the production of dry H_2 by electrolysis but could be favourable in a fuel-cell application where steam permeation from the cathode to the anode provides the water vapour for internal reforming of hydrocarbons [10]. Mapping of transport properties under a range of conditions is, therefore, most important for the further development of these promising materials in electrochemical applications.

The emf method for the determination of transport numbers in oxide-ion-conducting ceramics is fairly widely employed [11,12]. Electrode polarisation effects lead to a significant underestimation of the transport number of oxide-ion conductors by the emf method [13]. The Gorelov method of applying an external variable resistance in parallel with the cell, simulating the effect of enhanced electronic conductivity, provides a means of correcting for the polarisation resistance [13,14]. Very few works have applied the Gorelov method for the correction of proton transport numbers [15,16]. In this paper, we examine in more detail than these previous reports the emf technique for proton-transport determination and the application of the Gorelov (active-load) method

for the correction of electrode polarisation in the candidate PCEC and PCFC material $SrZr_{0.9}Y_{0.1}O_{3-\delta}$ with the addition of ZnO (4 mol.%) as sintering aid (SZY-Zn) [17] in wet oxidising conditions.

2. Theoretical

2.1. General aspects of the determination of transport numbers

In mixed-conducting oxides with several types of conducting species, it is practical to use the transport number of the corresponding species "j", defined as:

$$t_j = \frac{\sigma_j}{\sigma_{tot}} = \frac{\sigma_j}{\sum_j^n \sigma_j} = \frac{1/R_j}{\sum_j^n 1/R_j} \qquad (2)$$

where σ_j and σ_{tot} are the j carrier conductivity and total conductivity, respectively, and R_j is the resistance associated with the transport of the j carrier through the sample. It is apparent from Eq. 2 that

$$\sum_j^n t_j = 1 \qquad (3)$$

When the charge carriers are protons, oxide ions and electrons (or holes), the electrical transport through the sample can be represented by the equivalent circuit shown in Fig. 1(a); Eqs. 2 and 3 then yield

$$t_H = \frac{R_H^{-1}}{R_H^{-1} + R_O^{-1} + R_e^{-1}} = 1 - (t_e + t_O) = 1 - R_T\left(\frac{1}{R_e} + \frac{1}{R_O}\right) \quad (4)$$

and

$$t_O = 1 - R_T\left(\frac{1}{R_e} + \frac{1}{R_H}\right) \quad (5)$$

where subcripts H, O and e represent protons, oxide ions and electronic carriers, respectively, and R_T is the overall resistance of the sample (bulk + grain boundary). Moreover, the total ionic transport number is given by

$$t_{ion} = t_H + t_O = 1 - t_e = 1 - R_T\frac{1}{R_e} \quad (6)$$

The application of an external electric field to the sample produces a combined charge-transport process with parallel flows of charged species. As a consequence, the main conducting contribution prevails and minor components may be masked. Thus, the identification of each charge-transport component requires specific experimental methods. The emf method is based on the determination of the open-circuit voltage between two reversible electrodes of a mixed-conducting oxide exposed to a chemical potential gradient [11,12]. According to Eq. 2 and the model presented in Fig. 1(b), for a mixed-conducting sample with electronic carriers and generic ionic carriers, the ionic transport number averaged across the sample (t_{ion}) can be obtained by comparison between the observed electromotive force (E_{obs}) and the Nernst voltage (E_{Nernst}) as follows:

$$t_{ion} = \frac{R_e}{R_e + R_{ion}} = \frac{E_{obs}}{E_{Nernst}} \quad (7)$$

where the Nernst voltage corresponds to the theoretical open-circuit voltage for an ideal ionic conductor exposed to the same gradient of the active species [11,12,18,19]. When the concentration cell is submitted to a gradient of reactive gases of the active species, the Nernst voltage is expressed in terms of the partial pressures of the reacting gases as

$$E_{Nernst} = \frac{RT}{nF} \ln\left(\frac{p_1}{p_2}\right) \quad (8)$$

where R and T have their usual meanings, p_1 and p_2 are the partial pressures of the active gas at both surfaces of the ionic conductor, and n are the electrons transferred. However, Eq. 7 is derived under the assumption that interfacial processes are infinitely fast (Fig. 1(b)), thus limiting its use in real devices which are affected by interfacial overpotentials [20]. The influence of the electrode potential has been overlooked in many cases, mainly for mixed-conducting materials with the presence of protonic carriers [17,21], leading to the likelihood of large errors in the determination of the transport numbers.

A correct study of the transport properties of mixed-conducting oxides requires a methodology which marries both theoretical and practical approaches, as has been widely employed for mixed ionic-electronic conductors [13,20,22-24] and, of particular relevance to the present case, for mixed oxide-ionic-protonic-electronic conductors [15,16,25]. It has been demonstrated in the literature [26,27] that the presence of gradients of oxygen partial pressure (pO_2) and/or hydrogen partial pressure (pH_2) across these mixed conductors give rise to an electromotive force which, under the assumption

of non-polarisable electrodes, can be expressed in terms of the averaged protonic and oxide-ionic transport numbers as

$$E_{th} = \frac{RT}{4F} t_O \ln\left(\frac{pO_2'}{pO_2''}\right) - \frac{RT}{2F} t_H \ln\left(\frac{pH_2'}{pH_2''}\right) \quad (9)$$

In practical applications, however, it may be difficult to control both the oxygen and hydrogen partial pressures due to the equilibrium between hydrogen, oxygen and water vapour:

$$H_2 + \tfrac{1}{2} O_2 \rightleftarrows H_2O \quad (10)$$

Using this equilibrium, Eq. 9 is expressed in terms of oxygen partial pressure and water-vapour partial pressure (pH_2O) as

$$E_{th} = \frac{RT}{4F}\left(t_O + t_H\right) \ln\left(\frac{pO_2'}{pO_2''}\right) - \frac{RT}{2F} t_H \ln\left(\frac{pH_2O'}{pH_2O''}\right) \quad (11)$$

Equation 11 is a useful expression for oxidising conditions in which both pO_2 and pH_2O can be readily established.

Several equivalent circuits have been proposed to represent the mixed-conducting behaviour of a sample with simultaneous transport of several ionic and electronic species submitted to chemical potential gradients. Patterson [28] proposed the equivalent-circuit model presented in Fig. 2(a) for simultaneous transport of cationic, anionic and electronic species through a dense scale of a metal exposed to hostile gases

at high temperature. This model is also the basis adopted by Bentzer *et al.* [16] in a study of the emf technique for the determination of ionic transport number of $SrCe_{0.95}Y_{0.05}O_{3-\delta}$ under several working conditions, including the effect of the non-negligible polarisation at the electrodes. Alternatively, Frade [25] proposed a slightly different equivalent circuit, Fig. 2(b), the solution of which is in good agreement with the theoretically-deduced relation (Eq. 11), where

$$E_O = \frac{RT}{4F} \ln\left(\frac{pO_2'}{pO_2''}\right) \tag{12}$$

and

$$E_{H2O} = \frac{RT}{2F} \ln\left(\frac{pH_2O'}{pH_2O''}\right) \tag{13}$$

Nevertheless, both equivalent circuits presented in Fig. 2 lead to the same analytical solution if $R_1 = R_O$, $R_2 = R_H$, $R_3 = R_e$, $E_1 = E_O$ and $E_2 = -(E_{H2O}-E_O) = -E_{H2}$ [25]. This can be expressed in terms of the equilibrium between H_2, O_2 and H_2O (Eqs. 9 and 10), where

$$E_{H2} = \frac{RT}{2F} \ln\left(\frac{pH_2'}{pH_2''}\right) \tag{14}$$

2.2. Non-negligible electrode polarisation. Oxidising conditions.

In order to account for the possible impact of the electrode overpotentials on the measured open-circuit voltage, the relevant element should be incorporated in the equivalent circuit and the observed open-circuit voltage as a function of the

characteristic parameters should be determined. As both equivalent circuits presented in Fig. 2 fit conveniently to the theoretical formalism obtained from the electrochemical analysis (Eq. 11), both models could be considered as the basis for the development of our approach. Nevertheless, in the model presented in Fig. 2(a), the electromotive force E_2 is dependent on E_1. Moreover, the model presented in Fig. 2(b) better resembles our case in oxidising conditions given that the electromotive force corresponding to the protonic branch is directly related to the gradient in water-vapour partial pressure (Eq. 13). This allows both electromotive forces to be fixed in a simple manner under oxidising conditions by setting the values of pO_2 and pH_2O. The non-ideal, electrochemical-reaction kinetics at the interfaces are considered as resistive elements in series with the corresponding transport process of the ionic species (Fig. 3(a)).

It follows from Eq. 11 that the theoretical electromotive force of the mixed-conducting membrane submitted to a gradient in pH_2O with no gradient in pO_2 is directly related to t_H. Furthermore, the theoretical electromotive force is a function of $t_{ion}= t_O + t_H$ when there is a gradient in pO_2 but no gradient in pH_2O across the cell. Advantage can be taken of these relations for independent measurements of the electromotive force in order to derive the protonic and oxide-ionic transport numbers, as previously performed by some authors [15,16]. However, it is evident from Fig. 3(a) that the direct measurement of the electromotive force of the system (E_{obs}) differs considerably from the theoretical value (E_{th}) deduced from the electrochemical formalism presented in Eq. 11, due to the presence of the electrode-polarisation elements. This handicap is overcome by modification of the classical emf measurements via the introduction of an auxiliary parallel resistance [13].

2.2.1. Determination of protonic transport number (t_H).

In order to determine t_H, the same pO_2 is set at both sides of the sample, whereas a controlled gradient in pH_2O is established. In these circumstances, it follows from the equilibrium of Eq. 10 that

$$pO_2' \approx pO_2'' \tag{15}$$

and

$$\frac{pH_2'}{pH_2''} \approx \frac{pH_2O'}{pH_2O''} \tag{16}$$

As a consequence of the absence of a gradient in pO_2, the equivalent circuit representing the electrochemical system, Fig. 3(a), is considerably simplified by removing the dc source E_O and the polarisation resistance associated with the electrochemical reactions of oxidation-reduction of oxygen at the electrodes ($R_{\eta O}$). Modification of the emf measurements is performed by the introduction of a parallel variable resistance (R_{aux}), following the methodology widely developed for mixed ionic-electronic conducting oxides with a single ionic carrier [22,24] and recently adopted for oxide ionic-protonic-electronic conducting materials [15,16]. In these circumstances, the equivalent circuit corresponding to the whole system, including the auxiliary resistance, is presented in Fig. 3(b). Solving this circuit, it follows that

$$E_{obs}\left(\frac{1}{R_O}+\frac{1}{R_H+R_{\eta H}}+\frac{1}{R_e}+\frac{1}{R_{aux}}\right)=-E_{H2O}\,\frac{1}{R_H+R_{\eta H}} \tag{17}$$

and

$$\frac{-E_{H2O}}{E_{obs}}-1=\left(R_H+R_{\eta H}\right)\frac{1}{R_{aux}}+\left(\frac{1}{R_e}+\frac{1}{R_O}\right)\left(R_H+R_{\eta H}\right) \tag{18}$$

The factor $(-E_{H2O}/E_{obs})-1$ can be expressed as a linear function of $1/R_{aux,}$ $y=A_1x+B_1$, where

$$A_1 = \left(R_H + R_{\eta H}\right) \tag{19}$$

and

$$B_1 = \left(\frac{1}{R_e} + \frac{1}{R_O}\right)\left(R_H + R_{\eta H}\right) \tag{20}$$

The linear fitting of Eq. 18 for different values of external resistance provides a simple way to determine the protonic transport number averaged across the sample by combination of Eqs. 4, 19 and 20:

$$t_H = 1 - R_T\left(\frac{B_1}{A_1}\right) \tag{21}$$

where the overall resistance of the sample R_T (bulk + grain boundary) can be obtained on independent measurement by impedance spectroscopy in the same working conditions.

2.2.2. Determination of oxide-ionic transport number (t_O).

In this experiment, the same pH_2O as the average value employed in the previous experiment (subsection 2.2.1) is set on both sides of the cell. Similarly, the cell is submitted to a gradient of pO_2 whose average value also equals the constant value of

pO_2 fixed in the experiment outlined in subsection 2.2.1. We note that for small gradients of partial pressures of active species, the full behaviour of the electrochemical system is approximated by that of the average conditions. In this state, the modification of the emf methodology by the external resistance can be represented as shown in Fig. 3(c). From the current working conditions and the equilibrium of Eq. 10, it is inferred that

$$pH_2O' \approx pH_2O'' \tag{22}$$

and

$$\frac{pH_2'}{pH_2''} \approx \left(\frac{pO_2'}{pO_2''} \right)^{-1/2} \tag{23}$$

As pointed out by Sutija *et al.* [27], it is important to note that the presence of a gradient in pO_2 is sufficient to permeate protonic species from the lowest-pO_2 side to the highest-pO_2 side without the presence of a pH_2O gradient. We note that this is due to the existence of a gradient in pH_2. As a consequence, the contribution associated to the hydrogen oxidation-reduction reactions at the electrodes ($R_{\eta H}$) should be included in the equivalent circuit representing the whole electrochemical system (Fig. 3(c)). The solution of the circuit can be expressed as

$$E_{obs}\left(\frac{1}{R_e} + \frac{1}{R_{aux}} + \frac{1}{R_H + R_{\eta H}} + \frac{1}{R_O + R_{\eta O}} \right) = E_O \left(\frac{1}{R_H + R_{\eta H}} + \frac{1}{R_O + R_{\eta O}} \right) \tag{24}$$

giving

$$\frac{E_O}{E_{obs}} - 1 = \frac{\left(R_H + R_{\eta H}\right)\left(R_O + R_{\eta O}\right)}{\left(R_H + R_{\eta H}\right) + \left(R_O + R_{\eta O}\right)} \frac{1}{R_{aux}} + \frac{1}{R_e} \frac{\left(R_H + R_{\eta H}\right)\left(R_O + R_{\eta O}\right)}{\left(R_H + R_{\eta H}\right) + \left(R_O + R_{\eta O}\right)} \tag{25}$$

The solution of (E_O/E_{obs})-1 can thus be represented as a linear function of $1/R_{aux}$, $y=A_2x+B_2$, where

$$A_2 = \frac{\left(R_H + R_{\eta H}\right)\left(R_O + R_{\eta O}\right)}{\left(R_H + R_{\eta H}\right) + \left(R_O + R_{\eta O}\right)} \tag{26}$$

and

$$B_2 = \frac{1}{R_e}\frac{\left(R_H + R_{\eta H}\right)\left(R_O + R_{\eta O}\right)}{\left(R_H + R_{\eta H}\right) + \left(R_O + R_{\eta O}\right)} \tag{27}$$

From the linear fitting of Eq. 25 for different external resistance values (R_{aux}), combined with Eq. 6, it follows that

$$t_e = R_T\left(\frac{B_2}{A_2}\right) \tag{28}$$

and

$$t_O = 1 - R_T\left(\frac{B_2}{A_2}\right) - t_H \tag{29}$$

where t_H is determined as in section 2.2.1. The conductivity values associated with each species can then be determined from combination of Eqs. 2, 21, 28 and 29.

3. Experimental

Ceramic membranes of $Sr_{0.9}Y_{0.1}ZrO_{3-\delta}$ were prepared by solid-state reaction of $SrCO_3$ (99.9%, dried at 300 °C), ZrO_2 (99.7 % dried at 600 °C) and Y_2O_3 (dried at 950

°C) in the appropriate stoichiometric ratios, with the addition of 4 mol.% ZnO as sintering aid [17]. The reagents were attrition milled before heating slowly to 1100 °C for 12 hours to remove organic product and achieve improved homogenisation. Subsequent firing took place at 1250 °C for 24 hours with intermediate grinding in an agate mortar. This powder was then ball milled then re-milled with the addition of $Zn(NO_3)_2$, dried and sieved. Pellets of diameter 15 mm were formed on pressing the powder uniaxially prior to isostatic pressing to 190 MPa followed by sintering at 1500 °C for 6 hours.

Samples were examined for completeness of reaction and phase purity by powder X-ray diffraction (XRD) with a Bruker D8 high-resolution diffractometer equipped with a solid-state rapid LynxEye detector, using monochromatic $CuK\alpha_1$ radiation over the range $15° \leq 2\theta \leq 109°$. Lattice parameters were determined by Rietveld refinement using the Fullprof program [29]. The microstructure of a polished, thermally-etched transversal membrane surface was examined with Hitachi a TM-1000 tabletop scanning electron microscope. The densities of sintered pellets for electrical measurements were determined by careful measurement of the mass and geometrical volume; relative density was then calculated as a percentage of the theoretical X-ray density.

Electrodes were prepared by coating the pellets with Pt paste and firing at 900 °C for 1 hour in air to remove the organic content, harden the Pt and attach it to the pellet faces. Transport-number measurements were performed in a dual-chamber configuration by sealing the membrane to an yttria-stabilised zirconia (YSZ) tube with glass-ceramic sealant [30]. A schematic diagram of the measuring chamber is shown in Fig. 4. A paste of the powdered glass-ceramic in ethanol was applied between the outer wall of the open end of the tube and the disk; sealing was achieved on heating at 1

°Cmin^{-1} to 975 °C for a 10-minute dwell followed by cooling to the first measuring temperature. The inner and outer walls of the YSZ tube were coated with Pt electrodes close to the sample, and attached via Pt wires to a voltmeter for measurement of the pO_2 gradient across the sealed membrane.

The gas composition in the two chambers was controlled by a series of mass-flow controllers (Bronkhorst Hi-tec) for simultaneous control of pO_2 and pH_2O, Fig. 5, similar to the experimental set-up outlined by Sutija *et al.*[27]. Dry gases were fed through a drying column containing a moisture trap of aluminosilicate and zeolite-based beads (Supelco). Wet gases were fed through a humidifier consisting of a saturation stage followed by bubbling in a chamber with saturated KBr solution, which yields a water content of approximately 0.025 atm at room temperature [27]. The water content of this gas was then controlled by dilution with the dry gas, Fig. 5.

The ionic and electronic transport numbers were determined by the emf method in the temperature range 700-850 °C in a series of pH_2O and pO_2 gradients. The Gorelov (active-load) method of electrode-polarisation correction was applied by introducing a variable resistor, R_{aux} in parallel with the cell (Fig. 3). The thermovoltage contribution ($E_{thermal}$) to the measured electromotive force arising from slight gradients of temperature was taken into account by reversing the gas flow and measuring the actual values of emf under direct (E_{direct}) and reverse ($E_{reverse}$) flows, according to

$$E_{thermal} = \frac{E_{direct} + E_{reverse}}{2} \tag{30}$$

The effect of the thermovoltage was then eliminated as follows:

$$E_{obs} = E_{direct} - E_{thermal} \tag{31}$$

where E_{obs} corresponds to the electromotive force of the mixed conducting membrane, including electrode contribution, created by the chemical potential.

The sample resistance was determined by impedance spectroscopy in the frequency range $0.05 \leq f \leq 10^6$ Hz with an Autolab PGStat302N instrument operating in potentiostatic mode with a voltage amplitude of 250 mV. Impedance spectroscopy measurements were also performed in a single-atmosphere cell supplied with dry atmospheres of N_2, O_2 and air in the range 700–900 ºC.

4. Results and Discussion

4.1 Phase characterisation

The XRD powder pattern of $SrZr_{0.9}Y_{0.1}O_{3-\delta}$-4 mol.% ZnO sintered at 1500 °C for 6 h showed the formation of orthorhombically distorted perovskite , isostructural with $SrZrO_3$ (PDF. No. 44-0161), with lattice parameters a = 5.8216(2) , b = 8.2156(3), c = 5.8052(2) Å (space group, Pnma). No evidence of ZnO was apparent in the XRD pattern, although a small amount of SrY_2O_4 was identified. A similar result was reported by Peng *et al.* [17] for ZnO-modified SZY, who interpreted that Zn was located in the perovskite lattice; however, in this case Y_2O_3 was reported as a second phase. The effects of Zn on the phase composition, microstructure and transport properties of SZY in conditions relevant to electrochemical applications are currently under study in our group.

A scanning electron micrograph of a polished transversal surface, Fig. 6, reveals that the membrane is free of cracks and open porosity, with a grain size in the micron

range. Relative density was measured as, ~ 97 %, above the limit for gas tightness. The membrane maintained mechanical integrity throughout exposure to the experimental conditions.

4.2. Transport numbers in dry oxidising conditions

The electrical-transport properties of the SZY-Zn membrane were analysed under dry conditions on submitting the sample to a gradient of pO_2 without moistening. For this purpose, oxygen partial pressures of 0.3 atm and 0.1 atm were introduced in respective compartments by mixing flows of O_2 and N_2 with a total flow rate of 50 $ml \cdot min^{-1}$.

In this context, the material should be essentially free of protonic defects, the formation of which under oxidising conditions occurs by the hydration of oxygen vacancies according to Eq. (1). As a consequence, the protonic transport number is considered to be zero, and ionic transport process is solely assigned to oxide ions. This is a specific situation of the general case presented in Fig. 3(c) in which the protonic branch is removed (due to the protonic resistance approaching infinity) and the electromotive force derives from the pO_2 gradient (Eq. 12). The corresponding solution of the remaining equivalent circuit corresponds to the well-known solution for mixed oxide-ionic-electronic conductors [13,24]:

$$\frac{E_O}{E_{obs}} - 1 = \left(R_O + R_{\eta O}\right)\frac{1}{R_{aux}} + \frac{1}{R_e}\left(R_O + R_{\eta O}\right) \qquad (32)$$

We note that, although in dry conditions the pO_2 gradient may give rise to a pH_2O gradient according to Eq. 11 from the residual hydrogen present in air in the experimental starting conditions, the insignificant content of protonic species within the

material prevents an additional non-negligible contribution to the emf arising from any pH_2O gradient. Figure 7 shows the experimental data obtained for the SZY-Zn membrane by the Gorelov modification of the emf method in dry conditions at 850 ºC. The excellent fit of E_o/E_{obs}-1 to the linear dependence on $1000/R_{aux}$ for R_{aux} between 0.2–100 KΩ is apparent. The linear fitting parameters were combined with the overall resistance of the sample (R_T) determined from impedance spectroscopy to obtain the oxide–ionic and electronic transport numbers in the range 750–900 ºC, Fig. 8. The apparent oxide–ionic transport numbers ($t_{o,app}$) obtained without applying the active-load correction (Eq. 7), also shown in Fig. 8, deviate enormously from the corrected values due to the very high values of electrode polarisation, as observed by impedance spectroscopy (Fig. 9). The oxide-ionic conductivity under dry conditions is attributable to oxygen vacancies which are introduced on acceptor doping with Y^{3+} on the B position of $SrZrO_3$. A significant electron-hole contribution to transport was reported in $SrZrO_3$–based oxides doped with different trivalent cations on the Zr site, including Yb^{3+}, Y^{3+}, Ga^{3+}, Al^{3+} and In^{3+}, under dry oxidising conditions [31] according to the following equilibrium:

$$\frac{1}{2}O_2 + V_O^{\bullet\bullet} \rightleftarrows 2O_O^x + 2h^{\bullet} \qquad (33)$$

The presence of a significant electronic component to transport may also be attributable to the presence of ZnO, either incorporated in the perovskite structure, as was previously asserted by Peng *et al*. [17], or segregated in the grain boundaries. Although these authors reported that a quantity of ZnO less than 5 mol% does not significantly affect the electronic transport number in an emf measurement based on a fuel-cell configuration ($H_2/H_2O//O_2/H_2O$), in Peng *et al.'s* work, the behaviour in oxidising

conditions with the adoption of the Gorelov correction of electrode polarisation was not determined.

The presence of p-type transport is consistent with our results of total electrical conductivity under dry atmospheres of O_2, air and N_2 in the range 700–900 ºC, presented in Fig. 10, in which there is an increase in total conductivity when the sample is exposed to the more oxidising gases of air and O_2 in comparison to N_2. However, the dependence of conductivity on pO_2 deviates from a typical $\sigma \sim pO_2^{1/4}$ power-law dependence for dominating p-type transport carriers, suggesting that oxide-ions, in addition to electron holes, are responsible for electrical transport (Fig. 8).

It is also evident in Fig. 8 that the oxide-ionic transport number (t_O) increases and the electronic transport number (t_e) decreases with increasing temperature. This is a consequence of a lower activation energy for electronic conductivity compared with that of the oxide-ionic conductivity, as is observed in the Arrhenius representation of conductivity presented in Fig. 11.

4.3. Wet oxidising conditions.

Exposure of the sample to wet atmospheres under oxidising conditions creates protonic defects according to Eq. 1. The study of charge transport numbers was performed by independent experiments, as outlined in section 2. For the determination of t_H, the pO_2 was set to 0.2 atm in both compartments by mixing 10 ml·min^{-1} of O_2 with 40 ml·min^{-1} of N_2. A gradient of pH_2O was generated by exposing each side to a different level of dilution of dry and humidified O_2/N_2. As the experiments were restricted to relatively low gradients of pH_2O, the transport properties were analysed as functions of the average states. Figure 12 shows a representation of the modified

experimental emf data (Eq. 18) at 850 ºC in a pH_2O gradient of $2.4x10^{-2}/1.8x10^{-3}$ atm/atm. An excellent fit between the experimental data and the model in a wide range of values of auxiliary resistance (0.3-100 KΩ) can be observed. From the linear fitting parameters, t_H was obtained by combination with impedance-spectroscopy data according to Eq. 21. The t_H values as a function of the pH_2O averaged across the membrane for a fixed value of pO_2 = 0.2 atm at both sides of the sample are shown in Fig. 13. In the adopted wet conditions, the contribution to resistance from the electrode polarisation is significant, which is reflected as an appreciable voltage loss that lowers the observed electromotive force considerably and, as a consequence, gives very low values of apparent protonic transport number ($t_{H,app}$), according to Eq. 7. The protonic transport number increases with increasing pH_2O^{av}, in accordance with the higher concentration of protonic species (Eq. 1). Moreover, the absorption of protons is significantly higher at lower temperature, as is confirmed in Fig. 14 over a wider temperature range in different conditions of pH_2O^{av}, as a result of the exothermic hydration reaction, Eq. (1) [32]. It is notable that, on decreasing the temperature in the range 700-850 °C, the increase of protonic transport number is most significant from 750 °C to 700 °C. Recombination of total conductivity with the protonic transport number yields the protonic conductivity presented in Fig. 15(a). As is expected from the increase of t_H, the protonic conductivity increases for higher values of averaged pH_2O as a result of the higher concentration of protonic defects. Note that, in spite of the fact that the protonic transport number decreases with increasing temperature, the protonic conductivity increases at higher temperatures due to the higher proton mobility. According to the model outlined in subsection 2.2.1, recombination of Eqs. 19-20 allows the values of $\sigma_o + \sigma_e$ as a function of the averaged pH_2O, at a fixed pO_2 of 0.2 atm, to be calculated (Fig. 15(b)). Although the sum of $\sigma_o + \sigma_e$ is practically constant at

the higher range of pH_2O, a slightly greater value is obtained for this sum at the lowest measured pH_2O value.

For determination of $t_{ion} = t_H + t_O$, the sample was exposed to a gradient of pO_2 with the same level of humidification at both sides of the membrane. At this stage, the average conditions of partial pressures were chosen to be similar to those of the previous experiment in order to retain the average transport properties of the sample. In the present case, a pO_2^{av} of 0.2 atm was obtained by exposing one side of the sample to a mixture of O_2 and N_2 with flow rates of 15 and 35 $ml \cdot min^{-1}$, respectively, with the other side exposed to a mixture of 5 $ml \cdot min^{-1}$ of O_2 and 45 $ml \cdot min^{-1}$ of N_2. Gas mixtures at both sides were firstly wetted to the same degree of hydration on mixing gas (humidified with water at room temperature, followed by bubbling in a saturated KBr solution $pH_2O \sim 0.025$ atm) with the dry gas. Figure 16 shows a comparison of the protonic, oxide ionic, total ionic and electronic transport numbers at 750 ºC for different levels of humidification. The values of transport number previously obtained for "dry" conditions, assuming an estimated value of $pH_2O \approx 2x10^{-5}$ atm for our drying system, are also represented with data obtained under wet conditions. It is evident that the total ionic transport number is practically equal to the protonic transport number in the higher range of pH_2O, i.e. $t_O \approx 0$ and $\sigma_O \approx 0$. However, for $pH_2O \leq 3.8x10^{-3}$ atm, a significant increase of t_O accompanied by a decrease of t_H is observed on moving to drier conditions. Note that the total ionic transport number was assumed to be essentially equal to the oxide-ionic transport number under the dry conditions adopted in subsection 4.2. Figure 16 also shows a gradual increase of the electronic transport number as the water-vapour partial pressure decreases.

The conductivity associated to protons, oxide ions and electronic carriers, calculated from the transport numbers obtained by the modified emf technique and total

conductivity values, are represented as functions of the average water-vapour partial pressure in Fig. 17. It can be seen that the electronic conductivity is essentially constant, whereas the oxide-ionic conductivity increases by two orders of magnitude on moving to drier conditions in the range $2\times10^{-5} \leq pH_2O \leq 1.27x10^{-2}$, with a constant value of pO_2. These results are consistent with a charge-compensation mechanism in which the loss of protons is mainly balanced by the generation of oxygen vacancies according to Eq. 1. It follows that the equilibrium of Eq. 33 is essentially independent of the water-vapour partial pressure, in the studied range of wet conditions, due to the fixed value of pO_2 in these measurements. Our experimental results agree very well with the numerical solution of the defect equilibria reported by Bonanos *et al*. [33] of a generic proton-conducting perovskite, $AB_{1-y}M_yO_{3-\delta}$, where A and B represent cations with divalent and tetravalent oxidation states, respectively, and M represents a trivalent cation. The defect profiles obtained by these authors show a constant concentration of electronic defects, a considerable increase of oxygen vacancies and a less pronounced decrease of protons, with decreasing pH_2O in similar conditions to those employed in the current work. The changes in pH_2O^{av} should not affect any electronic transport component ascribable to ZnO, which may be segregated in grain boundaries.

5. Conclusions

An appropriate equivalent circuit was adopted for determination of proton, oxide-ion and electron transport numbers in the proton-conducting electrolyte material $SrZr_{0.9}Y_{0.1}O_{3-\delta}$-4 mol% ZnO with the inclusion of an external parallel resistance for correction of electrode polarisation. The modified methodology with the external parallel variable resistance yields significantly more accurate values of proton and

oxide-ion transport numbers, especially in the case of poor reaction kinetics at the electrodes.

Concentration cells with gradients in water-vapour partial pressure and fixed oxygen partial pressure were employed to determine proton transport numbers in wet oxidising conditions. Oxygen concentration cells with no gradient in pH_2O were employed to extract total ionic transport numbers, which were similar to protonic transport numbers in the higher range of pH_2O (> $3x10^{-3}$ atm), indicating negligible oxide- ionic conductivity. Progressing to drier conditions considerably increases the oxide-ionic transport number with a concomitant decrease of the protonic transport number. The electronic conductivity was practically independent of the water-vapour partial pressure, whereas the oxide-ionic conductivity increased by ~ two orders of magnitude when moving from the wetter to the drier conditions at the studied value of pO_2^{av}=0.2 atm. It is likely that electrolyser and fuel-cell operation parameters with $SrZr_{0.9}Y_{0.1}O_{3-\delta}$-4 mol% ZnO as electrolyte will be limited by significant electronic transport with increasing temperature and low water vapour partial pressures.

Acknowledgements

We thank the "Ministerio de Economía y Competitividad" (MINECO) (Plan Nacional, ENE2012-30929) for financial assistance. D. Pérez-Coll also acknowledges the support of a "Ramón y Cajal" contract (MINECO, CSIC). We are grateful to Dr M.J. Pascual (ICV, CSIC) for supplying the sealing glass-ceramic.

Figure Captions

Fig. 1. (a) Parallel transport of oxide ions, protons and electronic carriers through the mixed conducting sample submitted to an electrical field. (b) Equivalent circuit of a mixed-conducting sample with generic ionic and electronic carriers submitted to a chemical potential gradient of the active species under the ideal assumption that there is no polarization at the electrodes.

Fig. 2. (a) Equivalent-circuit model proposed by Patterson [28] for simultaneous transport of cationic, anionic and electronic species in a metal-dense scale under hostile gases and high temperature; (b) equivalent circuit model proposed by Frade [25] for a mixed conducting oxide with protons, oxide ions and electronic carriers submitted to gradients of water vapour and oxygen partial pressures.

Fig. 3. (a) Equivalent-circuit model considered in the current work for an oxide-ionic-protonic-electronic mixed conducting oxide submitted to gradients in pO_2 and pH_2O; (b) modification of the emf methodology by the introduction of an auxiliary parallel resistance for the electrochemical system exposed to a gradient in pH_2O without gradient in pO_2; (c) modification of emf for the electrochemical system submitted to a gradient in pO_2 without gradient in pH_2O.

Fig. 4. Schematic diagram of cell for determination of transport numbers. (1: alumina tube; 2.: thermocouple; 3: switch; 4: variable auxiliary resistance; 5: FRA; 6: voltmeter; 7: gas 1 inlet; 8: gas 2 inlet; 9: YSZ tube; 10: sealing glass-ceramic; 11: sample; 12: Pt electrodes; 13: Pt wires). Gas inlets/oulets are omitted for the sake of clarity.

Fig. 5. Schematic diagram of experimental set-up for supplying gas mixtures with controlled gradients of pO_2 and pH_2O across the membrane.

Fig. 6. Scanning electron micrograph of a polished and thermally-etched surface of the SZY-Zn membrane.

Fig. 7. Experimental data obtained by the active-load modification of the emf method for the sample exposed to a gradient of $pO_2'/pO_2'' = 0.3/0.1$ atm/atm under dry conditions at 850 ºC.

Fig. 8. Oxide-ionic and electronic transport numbers under dry conditions for a pO_2 gradient of 0.3/0.1 atm/atm in the range 750-900 ºC. The apparent ionic transport number obtained without modification of the emf method ($t_{o,app}$) is also shown for comparison.

Fig. 9. Impedance spectrum of the sample exposed to a dry gradient $pO_2'/pO_2'' = 0.3/0.1$ atm/atm at 900 ºC.

Fig. 10. Arrhenius representation of total conductivity of the sample submitted to single atmospheres of dry O_2, air and N_2.

Fig. 11. Arrhenius representation of oxide-ionic, electronic and total conductivities under dry conditions in a pO_2 gradient of 0.3/0.1 atm/atm.

Fig. 12. Experimental data of emf measurements at 850 ºC after Gorelov's modification at fixed $pO_2 = 0.2$ atm and under a pH_2O gradient of $2.4x10^{-2}/1.8x10^{-3}$ atm/atm.

Fig. 13. Protonic transport number averaged across the membrane as a function of the average pH_2O at 700 ºC and 850 ºC. The sample was exposed to several gradients of pH_2O in the absence of a pO_2 gradient. The apparent protonic transport numbers obtanied without modification of the emf methodology are also represented for comparison.

Fig. 14. Average protonic transport number as a function of temperature for sample exposed to different pH_2O in the absence of a pO_2 gradient.

Fig. 15. (a) Protonic conductivity as a function of the pH_2O averaged across the membrane without pO_2 gradient; (b) sum of oxide-ionic and electronic conductivities versus average pH_2O.

Fig. 16. Total ionic, protonic, oxide ionic and electronic transport numbers as functions of water partial pressure averaged across the membrane at 750 ºC. The lowest value of water partial pressure corresponds to “dry” conditions and was estimated as $3x10^{-5}$ atm.

Fig. 17. Logartihmic representation of conductivity associated to protons, oxide ions and electronic carriers versus water partial pressure for an average oxygen partial pressure of 0.2 atm.

References

[1] L. Shaw, J. Pratt, L. Klebanoff, T. Johnson, M. Arienti, M. Moreno, Int. J. Hydrog. Energy 38 (2013) 2810-2823.

[2] B.D. Solomon, A. Banerjee, Energy Policy 34 (2006) 781-792.

[3] B. Johnston, M.C. Mayo, A. Khare, Technovation 25 (2005) 569-585.

[4] R. Farrauto, S. Hwang, L. Shore, W. Ruettinger, J. Lampert, T. Giroux, Y. Liu, O. Ilinich, Ann. Rev. Mater. Res. 33 (2003) 1-27.

[5] T. Sakai, S. Matsushita, H. Matsumoto, S. Okada, S. Hashimoto, T. Ishihara, Int. J. Hydrog. Energy 34 (2009) 56-63.

[6] H. Matsumoto, T. Shimura, H. Iwahara, T. Higuchi, K. Yashiro, A. Kaimai, T. Kawada, J. Mizusaki, J. Alloys Compd. 408-412 (2006) 456-462.

[7] K. D. Kreuer, Solid State Ionics 97 (1997) 1-15.

[8] K. D. Kreuer, Ann. Rev. Mater. Res. 33 (2003) 333-359.

[9] W.G. Coors, Solid State Ionics 178 (2007) 481-485.

[10] W.G. Coors, J. Power Sources 118 (2003) 150-156.

[11] H. Yahiro, Y. Baba, K. Eguchi, H. Arai, J. Electrochem. Soc. 135 (1988) 2077-2080.

[12] N. Bonanos, B. Ellis, K.S. Knight, M.N. Mahmood, Solid State Ionics 35 (1989) 179-188.

[13] V.V. Kharton, F.M.B. Marques, Solid State Ionics 140 (2001) 381-394.

[14] V.P. Gorelov, Elektrokhimiya 24 (1988) 1380 (in Russian)

[15] A.D. Brandão, I. Antunes, J.R. Frade, J. Torre, V.V. Kharton, D.P. Fagg, Chem. Mater. 22 (2010) 6673-6683.

[16] H. Bentzer, N. Bonanos, J.W. Phair, Solid State Ionics 181 (2010) 249-255.

[17] Z. Peng, R. Guo, Z. Yin, J. Li, J. Am. Ceram. Soc. 91 (2008) 1534-1538.

[18] H. Iwahara, Solid State Ionics 52 (1992) 99-104.

[19] H. Iwahara, H. Uchida, N. Maeda, Solid State Ionics 11 (1983) 109-115.

[20] M. Liu, H. Hu, J. Electrochem. Soc. 143 (1996) L109-L112.

[21] P. Babilo, S.M. Haile, J. Am. Ceram. Soc. 88 (2005) 2362-2368.

[22] J.R. Frade, V.V. Kharton, A.A. Yaremchenko, E.V. Tsipis, J. Solid State Electrochem. 10 (2006) 96-103.

[23] J.R. Jurado, F.M. Figueiredo, J.R. Frade, Solid State Ionics 122 (1999) 197-204.

[24] V.V. Kharton, A.P. Viskup, F.M. Figueiredo, E.N. Naumovich, A.A. Yaremchenko, F.M.B. Marques, Electrochim. Acta 46 (2001) 2879-2889.
[25] J.R. Frade, Solid State Ionics 78 (1995) 87-97.
[26] T. Norby, Solid State Ionics 28-30 (1988) 1586-1591.
[27] D.P. Sutija, T. Norby, P. Björnbom, Solid State Ionics 77 (1995) 167-174.
[28] J.W. Patterson, Ind. Eng. Chem. Prod. Res. Dev. 17 (1978) 19-24.
[29] J. Rodríguez-Carvajal, Physica B 192 (1993) 55-69.
[30] M.J. Pascual, A.Guillet, A.Durán, J. Power Sources 169 (2007) 40-46.
[31] T. Yajima, H. Suzuki, T. Yogo, H. Iwahara, Solid State Ionics 51 (1992) 101-107.
[32] R. Haugsrud, T. Norby, Nat. Mater. 5 (2006) 193-196.
[33] N. Bonanos, F.W. Poulsen, J. Mater. Chem. 9 (1999) 431-434.

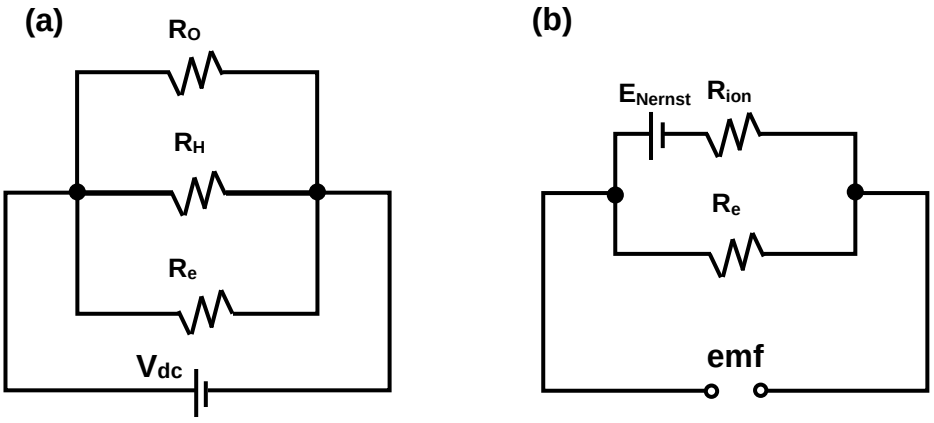

Fig. 1.

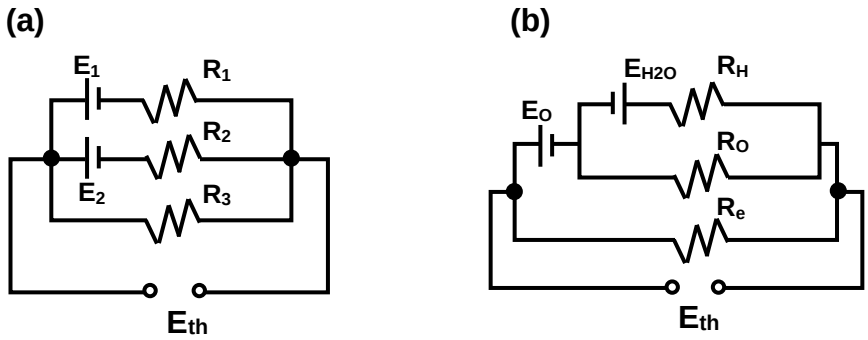

Fig. 2.

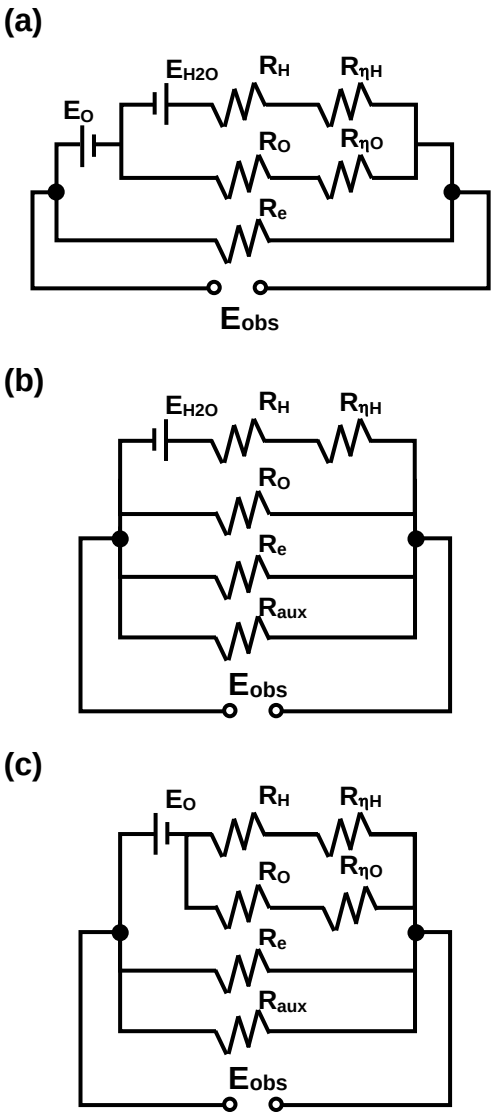
(a)
E_{H2O}
R_H
$R_{\eta H}$
E_O
R_O
$R_{\eta O}$
R_e
E_{obs}
(b)
E_{H2O}
R_H
$R_{\eta H}$
R_O
R_e
R_{aux}
E_{obs}
(c)
E_O
R_H
$R_{\eta H}$
R_O
$R_{\eta O}$
R_e
R_{aux}
E_{obs}

Fig. 3.

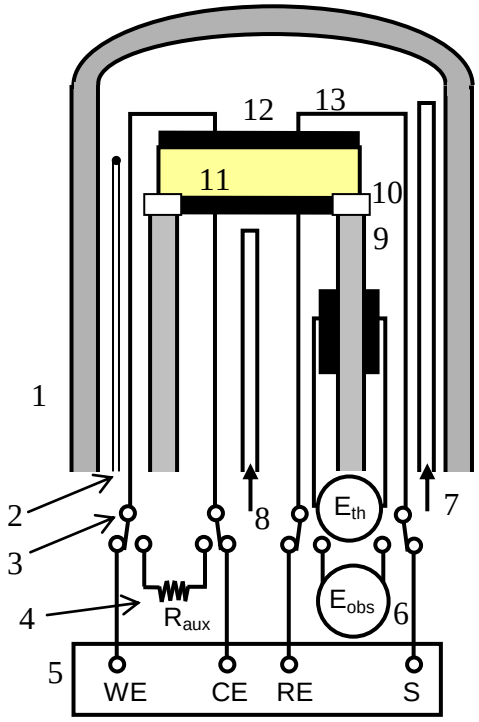

Fig. 4.

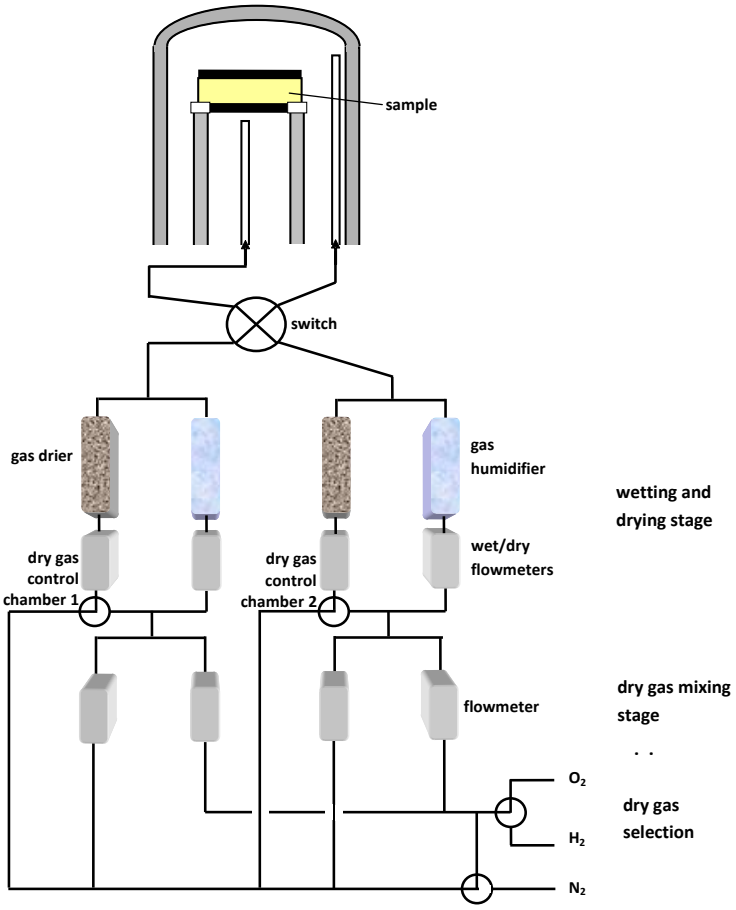
sample
switch
gas drier
gas humidifier
wetting and drying stage
dry gas control chamber 1
dry gas control chamber 2
wet/dry flowmeters
flowmeter
dry gas mixing stage
. .
O_2
H_2
N_2
dry gas selection

Fig. 5.

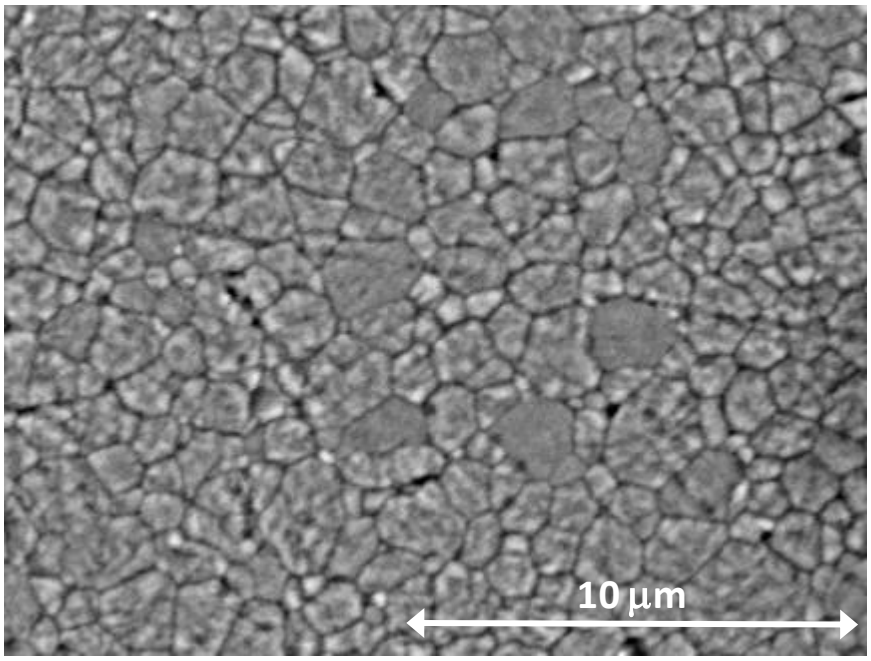

Fig. 6.

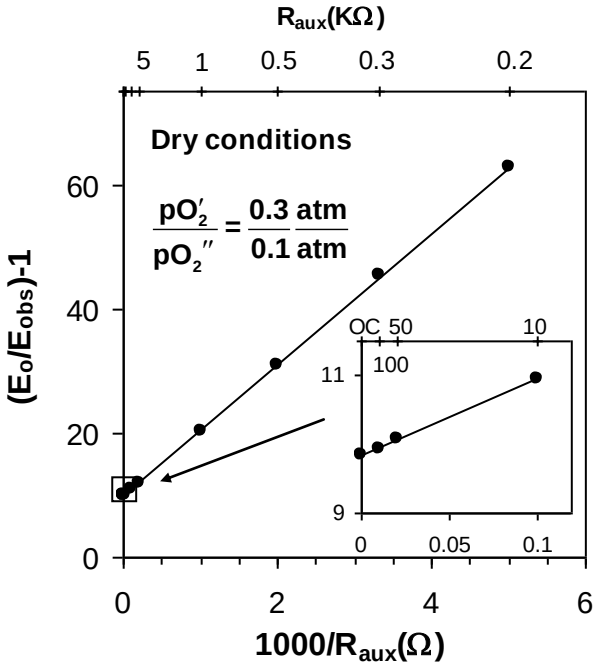
R_aux(KΩ)
5
1
0.5
0.3
0.2
Dry conditions
pO'2 / pO2'' = 0.3 atm / 0.1 atm
(Eo/Eobs)-1
60
40
20
0
OC
50
10
100
11
9
0
0.05
0.1
0
2
4
6
1000/Raux(Ω)

Fig. 7.

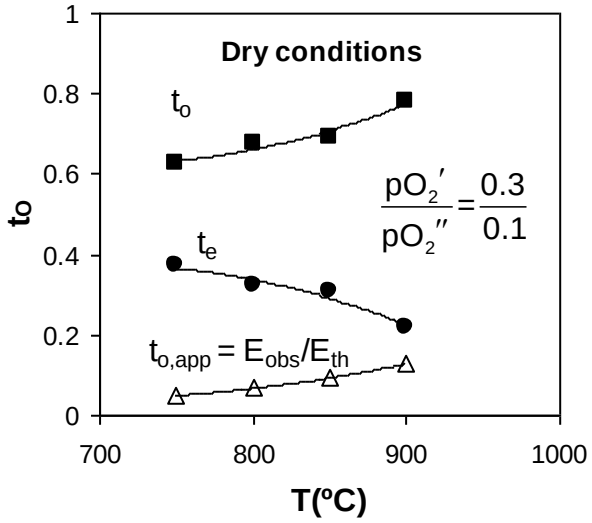
Dry conditions
t_o
t_e
$t_{o,app} = E_{obs}/E_{th}$
$\frac{pO_2'}{pO_2''} = \frac{0.3}{0.1}$
t_o
T(ºC)
1
0.8
0.6
0.4
0.2
0
700
800
900
1000

Fig. 8.

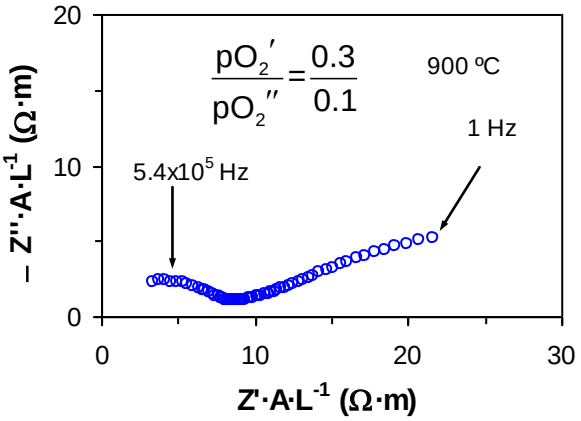
20
10
0
0
10
20
30
– Z''·A·L-1 (Ω·m)
Z'·A·L-1 (Ω·m)
pO2′ / pO2″ = 0.3 / 0.1
900 ºC
1 Hz
5.4x10^5 Hz

Fig. 9.

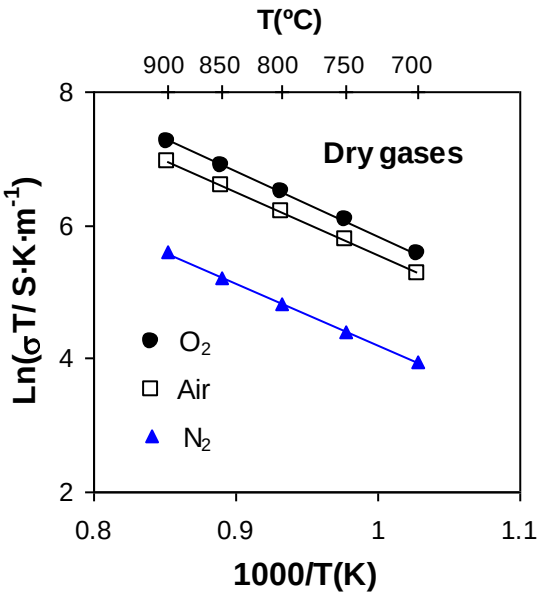
T(°C)
900 850 800 750 700
8
6
4
2
Ln(σT/ S·K·m-1)
Dry gases
O2
Air
N2
0.8
0.9
1
1.1
1000/T(K)

Fig. 10.

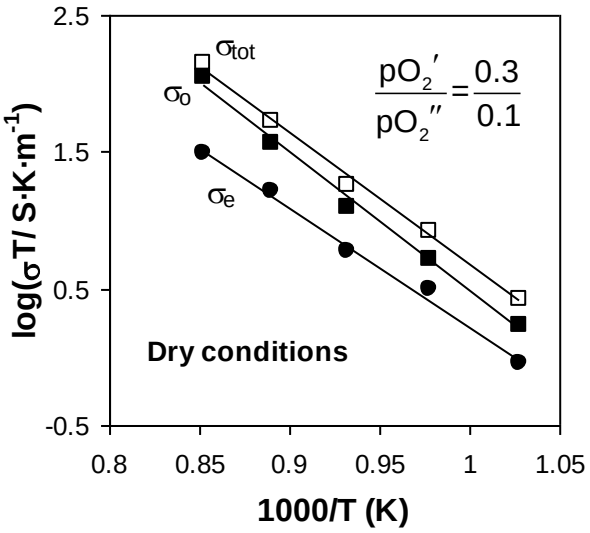
2.5
1.5
0.5
-0.5
0.8
0.85
0.9
0.95
1
1.05
log(σT/ S·K·m-1)
1000/T (K)
σtot
σo
σe
pO2′ / pO2″ = 0.3 / 0.1
Dry conditions

Fig. 11.

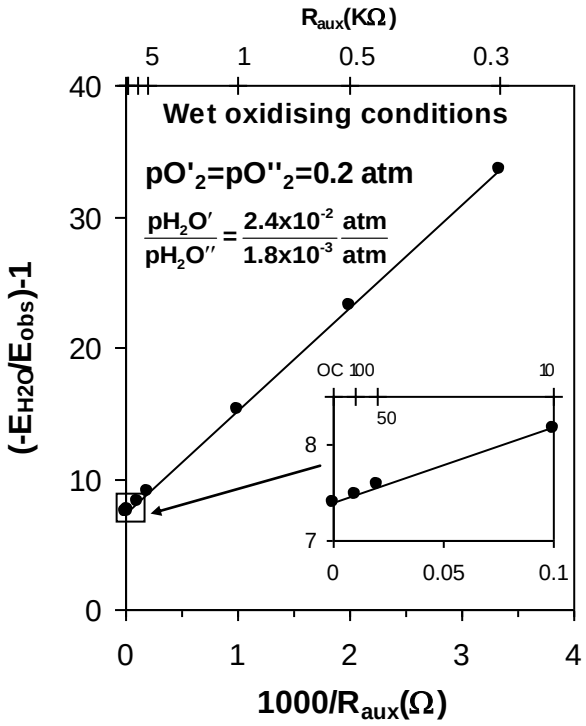
R_aux(KΩ)
5
1
0.5
0.3
40
30
20
10
0
Wet oxidising conditions
pO'2=pO''2=0.2 atm
pH2O′ / pH2O″ = 2.4x10-2 atm / 1.8x10-3 atm
(-EH2O/Eobs)-1
OC
100
50
10
8
7
0
0.05
0.1
0
1
2
3
4
1000/Raux(Ω)

Fig. 12.

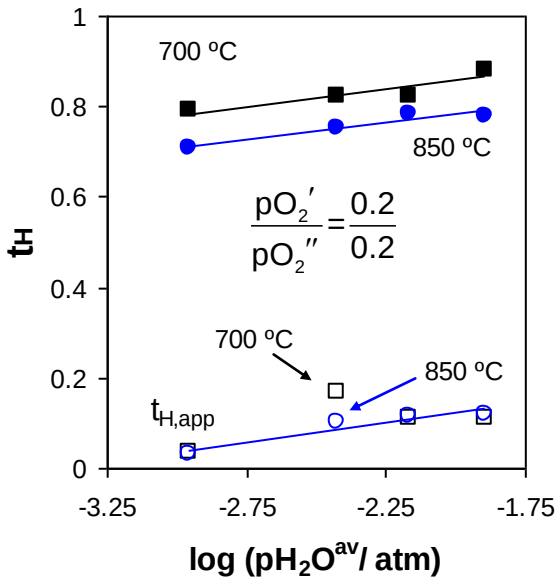
1
0.8
0.6
0.4
0.2
0
t_H
700 ºC
850 ºC
$\frac{pO_2'}{pO_2''} = \frac{0.2}{0.2}$
700 ºC
850 ºC
$t_{H,app}$
-3.25
-2.75
-2.25
-1.75
log (pH_2O^{av}/ atm)

Fig. 13.

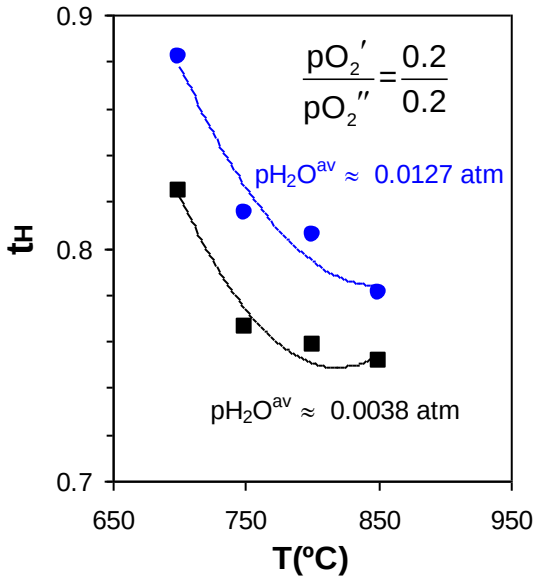
0.9
0.8
0.7
650
750
850
950
T(ºC)
tH
pO2′ / pO2″ = 0.2 / 0.2
pH2Oav ≈ 0.0127 atm
pH2Oav ≈ 0.0038 atm

Fig. 14.

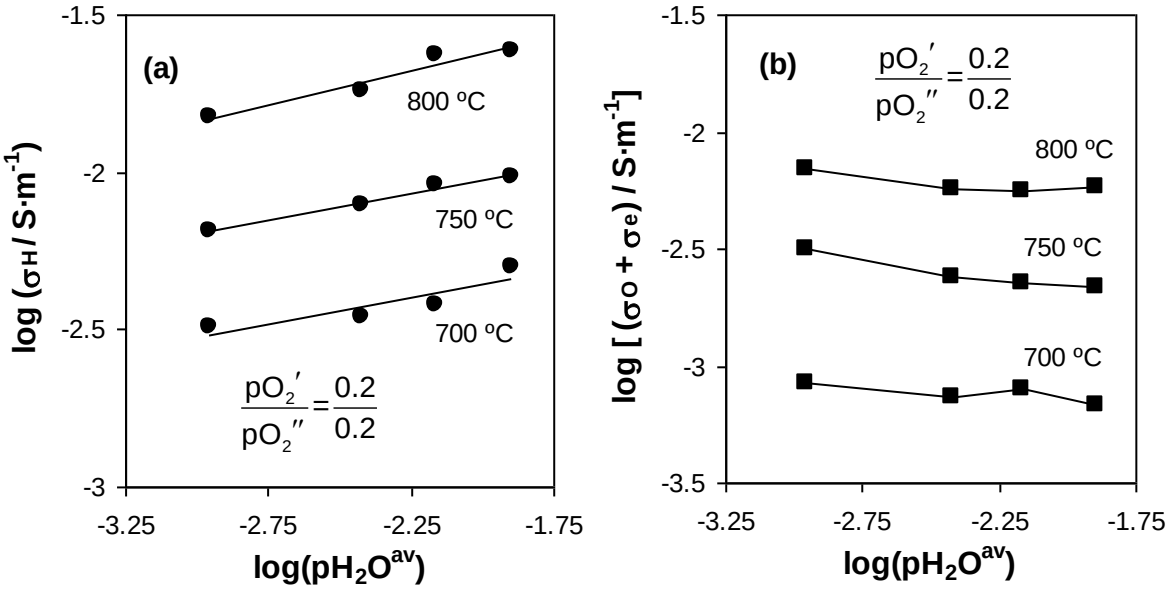
(a)
800 ºC
750 ºC
700 ºC
$\frac{pO_2'}{pO_2''} = \frac{0.2}{0.2}$
log (σH / S·m-1)
log(pH2Oav)
-1.5
-2
-2.5
-3
-3.25
-2.75
-2.25
-1.75
(b)
$\frac{pO_2'}{pO_2''} = \frac{0.2}{0.2}$
800 ºC
750 ºC
700 ºC
log [(σO + σe) / S·m-1]
log(pH2Oav)
-1.5
-2
-2.5
-3
-3.5
-3.25
-2.75
-2.25
-1.75

Fig. 15.

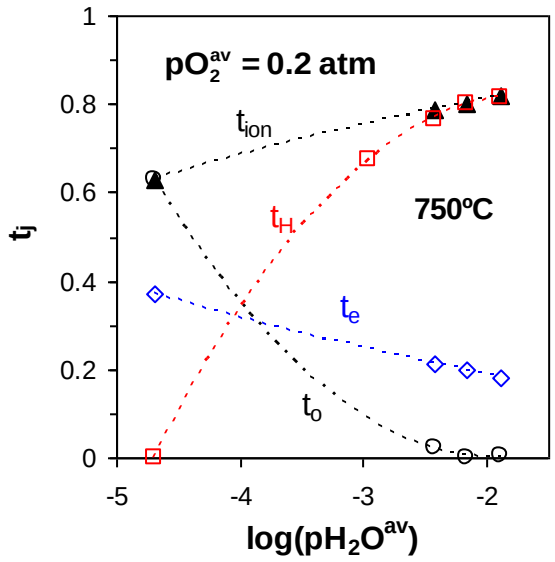
1
0.8
0.6
0.4
0.2
0
-5
-4
-3
-2
t_j
pO_2^{av} = 0.2 atm
t_{ion}
t_H
t_e
t_o
750ºC
$\log(pH_2O^{av})$

Fig. 16.

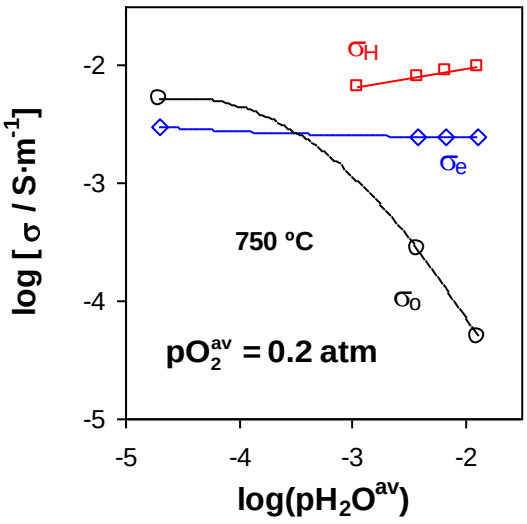

Fig. 17.